Atmos. Chem. Phys. Discuss., 12, 5293–5340, 2012
www.atmos-chem-phys-discuss.net/12/5293/2012/
doi:10.5194/acpd-12-5293-2012

Atmospheric Chemistry and Physics Discussions

Aerosol hygroscopicity at Ispra EMEP-GAW station

M. Adam, J. P. Putaud, S. Martins dos Santos, A. Dell'Acqua, and C. Gruening

European Commission, Joint Research Centre, 21027, Ispra, Italy

Received: 16 December 2011 – Accepted: 30 January 2012 – Published: 17 February 2012

Correspondence to: J. P. Putaud (jean.putaud@jrc.ec.europa.eu)

Published by Copernicus Publications on behalf of the European Geosciences Union.

Abstract

This study focuses on the aerosol hygroscopic properties as determined from ground-based measurements and Mie theory. Usually, aerosol ground-based measurements are taken in dry conditions to ensure data consistency within networks. The dependence of the various aerosol optical characteristics (e.g. aerosol absorption, scattering, backscattering or extinction coefficients) on relative humidity has therefore to be established in order to determine their values in the atmosphere, where relative humidity can reach high values.

We calculated mean monthly diurnal values of the aerosol hygroscopic growth factor at 90 % relative humidity GF(90) based on measurements performed at EMEP-GAW station of Ispra with a Hygroscopicity Tandem Differential Mobility Analyzer over eight months in 2008 and 2009. Particle hygroscopicity increases with particle dry diameter ranging from 35 to 165 nm for all seasons. We observed a clear seasonal variation in GF(90) for particles larger than 75 nm, and a diurnal cycle in spring and winter for all sizes. For 165 nm particles, GF(90) averages 1.32 ± 0.06.

The effect of the particle hygroscopic growth on the aerosol optical properties (scattering, extinction, absorption and backscatter coefficients, asymmetry parameter and backscatter faction) was computed using the Mie theory, based on data obtained from a series of instruments running at our station. We found median enhancement factors (defined as ratios between the values of optical variables at 90 % and 0 % relative humidity) equal to 1.1, 2.1, 1.7, and 1.8, for the aerosol absorption, scattering, backscattering, and extinction coefficients, respectively. All except the absorption enhancement factor show a strong correlation with the hygroscopic growth factor. The enhancement factors observed at our site are among the lowest observed across the world for the aerosol scattering coefficient, and among the highest for the aerosol backscatter fraction.

ACPD
12, 5293–5340, 2012

1 Introduction

Atmospheric aerosol particles reveal changes in their microphysical and optical properties with relative humidity (RH) due to the water uptake. These changes depend on the particles' chemical composition and size. In situ measurements of the particles physical and optical properties usually take place in low RH conditions (RH < 20–30 %), in order to have consistent data within measurement networks. In order to determine the properties of the aerosol in ambient conditions, corrections have to be applied to all the parameters measured in dry conditions. These corrections are mandatory once we need to compare these in-situ measurements with other measurements taken at ambient conditions (e.g. from satellite-borne or ground-based active or passive remote sensing devices). Moreover, the aerosol optical parameters (aerosol scattering, absorption and backscatter coefficient) at ambient RH represent the input to the radiative transfer models to determine the direct aerosol climate forcing (e.g. Chylek and Wong, 1995).

The main parameter used to characterize the change in the microphysical properties of the particles is the hygroscopic growth factor GF(RH), which is defined as the ratio of the particle diameter at any RH to the particle diameter at RH = 0 %. This factor can be measured by a Hygroscopicity Tandem Differential Mobility Analyzer (HTDMA). The resulting change in the optical properties is described by the enhancement factor f(RH), which, for a specific optical parameter χ, is defined as the ratio between its values determined in any conditions χ(RH) and to those determined in dry conditions χ(RH = 0 %). Technically, the enhancement factor for scattering and hemispherical backscattering can be determined for a chosen RH by using two nephelometers performing measurements at the chosen RH and in dry conditions (RH = 0 %), respectively.

In this study, the results of the measurements taken by a HTDMA over eight months during 2008 and 2009 are used to obtain a climatology of the hygroscopic growth factor GF(RH). This is used to estimate the enhancement factors for various aerosol optical properties (scattering, backscattering, absorption coefficients, and asymmetry

ACPD
12, 5293–5340, 2012

parameter), derived from measurements taken at our station in Ispra (Italy), and the Mie theory (Van del Hust, 1981; Bohren and Hofmann, 1998). Briefly, the hygroscopic growth factor measured at 90 % relative humidity is used to derive the particles growth over the entire relative humidity range. The monthly diurnal growth factor is then employed to correct the particle size distribution and optical properties to dry (0 % RH) and ambient conditions. The strong correlation between growth factor and enhancement factors will allow us to correct the measurements (taken at the instrument's RH conditions) to dry or ambient conditions, as far as RH in the instrument is known.

The paper shortly presents the EMEP-GAW station in Ispra (Sect. 2). The methodologies to determine the hygroscopic growth factor and the enhancement factors are described in Sect. 3. In Sect. 4, we present and discuss results, assess uncertainties and compare the aerosol characteristics at our site with others. Conclusions highlight how our results can be used for other locations, considering the specificities of the aerosol at our site (Sect. 5).

2 The EMEP-GAW regional station in Ispra

The JRC station for atmospheric research (45°48.881′ N, 8°38.165′ E, 209 m a.s.l.) is situated in a semi-rural area at the NW edge of the Po valley in Italy. The station is several tens of km away from large emission sources like intense road traffic or big factories. The aim of the JRC-Ispra station is to monitor the concentration of pollutants in the gas phase, the particulate phase and precipitations, as well as aerosol optical properties, which can be used for assessing the impact of European policies on air pollution and climate change. Measurements are performed in the framework of international monitoring programs like the *Co-operative program for monitoring and evaluation of the long range transmission of air pollutants in Europe (EMEP)* of the UN-ECE *Convention on Long-Range Transboundary Air Pollution (CLRTAP)* and the *Global Atmosphere Watch (GAW)* program of the World Meteorological Organization (WMO). The JRC-Ispra station operates on a regular basis in the extended EMEP

ACPD
12, 5293–5340, 2012

measurement program since November 1985. Aerosol physical and optical properties have been monitored since November 2003. The station has been favorably audited by the World Calibration Centre for Aerosol Physics (WCCAP) in March 2010.

The particle number size distribution is measured continuously with a home-made (Vienna type) Differential Mobility Particle Sizer (DMPS) between 10 and 600 nm mobility diameter, and an Aerodynamic Particle Sizer (APS – TSI 3321) between 0.720 to 12.0 µm aerodynamic diameter. Mobility and aerodynamic diameters were converted to geometric diameters assuming that particles are spherical and their density is 1.5. The aerosol scattering and backscatter coefficients are measured with an integrating Nephelometer (TSI 3753) at 450, 550 and 700 nm. Nephelometer data were corrected for angular non idealities and truncation errors according to Anderson and Ogren (1998). The aerosol absorption coefficient at 450, 550 and 700 nm are derived from 7-wavelength Aethalometer (Magee AE31) data, using a scheme based on Weingartner et al. (2003), with correction coefficients estimated from Schmid et al. (2006). Data are transmitted yearly to the EBAS data bank (http://ebas.nilu.no/). A technical report of the station is internally published each year (e.g. Jensen et al., 2009).

From May 2008 to April 2009, a coordinated action to measure the aerosol hygroscopic growth factor (by means of HTDMA instruments) over the four seasons took place within the EU-funded EUSAAR (European Supersites for Atmospheric Aerosol Research) project (www.eusaar.net). Eleven stations participated in this activity (Vavihill, Puy de Dome, Jungfraujoch, Ispra, Cabauw, Melpitz, Hyytiälä, Mace Head, Pallas, Kosetice, and Harwell) and the general results will be published soon in a common paper (Swietlicki et al., 2012), focusing on the European phenomenology of the aerosol hygroscopicity properties. The results obtained at the Ispra site are briefly discussed within Sect. 4.1, and further exploited to calculate enhancement factors in Sect. 4.2.

ACPD
12, 5293–5340, 2012

3 Methodology

The aerosol hygroscopic growth factor is analyzed through the measurements taken by the home-made HTDMA (Duplissy et al., 2009). A short description of the growth factor determination is outlined in Sect. 3.1.

The effect of RH on the aerosol optical properties is studied by the means of enhancement factors. The methodology employed to determine these factors, is presented in Sect. 3.2.

3.1 Hygroscopic growth factor

The first measurements of particle hygroscopic growth factor performed with the Ispra custom-made HTDMA were carried out during the 90'. The system description and some results can be found in Virkkula et al. (1999) and Van Dingenen et al. (2005). During summer 2006 and winter 2007, an intercomparison campaign took place at Paul Scherrer Institute in Switzerland, where six HTDMA were compared, including the Ispra instrument (Duplissy et al., 2009). The experiment focused on the methods of calibration, validation and data analysis. Measurements of ammonium sulphate and secondary organic aerosol were performed. All HTDMAs confirmed the sizing stability within ±1 % and RH stability under constant laboratory temperature conditions within less than ±2 %. However, systematic measurement errors were observed during variable laboratory temperature conditions for our HTDMA. The humidogram of pure ammonium sulphate exhibited some −5.6 % difference in GF at 85 % with respect to the literature (Topping et al., 2005). The specific set-up of our instrument, including the locations of RH monitoring probe was the main cause of the discrepancies. Following this intercomparison exercise, the instrument did not undergo changes or upgrades, but during April 2009, a series of humidograms were measured for ammonium sulphate. The mean growth factor at 110 nm showed a value of 1.60, i.e. 3.5 % smaller than the literature value of 1.66. It is therefore possible that the growth factor we measured were underestimated by 3.5 %.

ACPD
12, 5293–5340, 2012

Our HTDMA provided data for the aerosol hygroscopic factor at 90 % RH for five dry diameters: 35, 50, 75, 110 and 165 nm. The GF probability density function (GF-PDF) are determined following the procedure developed by Gysel et al. (2009), using the TDMAInv toolkit. Note that in cases when the target RH (90 %) is not accomplished, an empirical correction is applied to the measured GFs and GF-PDFs (Gysel et al., 2009). Shortly, the philosophy behind this procedure is as follows. The measured GF distribution function (MDF) is an integral transform of the particle's actual GF-PDF. Thus, an inversion algorithm is applied to MDF to retrieve the GF-PDF. Further, the mean GF of the sample and the number fractions of particles in different GF ranges are determined.

$$\langle \mathrm{GF} \rangle = \int_0^\infty \mathrm{GF} \cdot \mathrm{GFPDF} d\mathrm{GF} \tag{1}$$

$$\mathrm{NF}^{a,b} = \int_a^b \mathrm{GFPDF} d\mathrm{GF}. \tag{2}$$

For more details, please see Gysel et al. (2009) and the inversion toolkit (http://people.web.psi.ch/gysel).

3.2 Enhancement factors

Enhancement factors can be defined for each of the optical variables such as: aerosol scattering, aerosol absorption, aerosol extinction or aerosol backscattering coefficients. We have also applied the enhancement factor terminology for the asymmetry parameter. In general, the enhancement factor can be defined as:

$$f_\chi(\mathrm{RH}, \lambda) = \frac{\chi(\mathrm{RH}, \lambda)}{\chi(\mathrm{RH} = 0, \lambda)}. \tag{3}$$

where χ can be σ, α, κ, β, g, or bf, denoting the aerosol scattering, absorption, extinction, backscatter coefficient, asymmetry parameter or backscatter fraction, respectively. RH corresponds to the any conditions, which can cover the entire RH spectrum. The

ACPD
12, 5293–5340, 2012

most employed is the scattering enhancement factor and this is due to the fact that it can be directly determined from nephelometers measurements.

Alternatively, f_χ can be calculated using the Mie theory if the aerosol refractive index and GF(RH) are known, and assuming an aerosol internal mixture. The latter assumption allows us to calculate the refractive index of wet particles as a volume weighted average of the refractive indices of the dry aerosol and water. Thus, the mentioned optical properties at any RH condition can be related to those at RH = 0 %. The flow chart of this procedure is shown in Fig. 1. The input data are the aerosol hygroscopic factor at RH = 90 % for d_{dry} = 165 nm provided by the HTDMA, the particle number size distribution over the range 10 nm–10 µm at RH < 30 %, the aerosol scattering and absorption coefficient at 450, 550 and 700 nm at RH < 35 %. The outputs are the enhancement factors of the optical variables. We determine also the asymmetry parameter g (Mie theory), and its enhancement factor. For comparison purposes, we also estimate the asymmetry parameter g_{neph} for the nephelometer RH conditions (i.e. not in dry conditions) from the measured backscatter fraction and an empirical formula developed by Arnott (Andrews et al., 2006).

Note that we use monthly diurnal averages GF at d_{dry} = 165 nm only. This option is supported by the fact that particles larger than 165 nm interact more efficiently with visible light (Fig. 2). The particles around 600–750 nm have the largest scattering and extinction efficiency (ξ), and although the largest particle number concentration (N) is around 100 nm, the largest contribution to scattering ($N \cdot \xi$) is around 200–300 nm. Thus, using GF for d_{dry} = 165 nm also for smaller particles, practically does not affect enhancement factors. This approach was also used in earlier studies (e.g. Zieger et al., 2010). However, particles larger than 165 nm might have a different GF, due to a different chemical composition. This issue is further discussed in Sect. 4.3.1.

GF(RH) is determined using a γ-model (e.g. Kasten, 1969; Gysel et al., 2009):

$$\mathrm{GF(RH)} = \left(1 - {}^{\mathrm{RH}}/_{100}\right)^{-\gamma}. \quad (4)$$

where γ is determined from boundary condition at RH = 90 %.

ACPD
12, 5293–5340, 2012

The main unknown variable when applying Mie theory is the aerosol refractive index. This was determined from the closure of the measured with computed (Mie) aerosol scattering and absorption coefficients. Note that this refractive index corresponds to instrument conditions such that we denote it as m_{inst}. The measured aerosol scattering and absorption coefficients at 450, 550, and 700 nm are compared with a lookup table of the computed aerosol scattering and absorption efficiencies. The calculated coefficients employ the measured NSD and particles diameters at instruments RH conditions. That is why these computations were performed only when the absolute difference in RH between the instrument measuring the particle number size distribution and the optical parameters was below 5 %. The wavelengths considered are 450, 550 and 700 nm. For the lookup table, the refractive index covers the range from 1.3 to 1.7 (with 0.01 step) for the real part and the range from 0 to 0.6 (with 0.001 step) for the imaginary part. Note that no dispersion for the refractive index was considered over the three wavelengths. This is a common assumption for the visible spectrum (e.g. Adam et al., 2004; Nessler et al., 2005a, b; Zieger et al., 2010, 2011). The match with measurements is given by the smallest (overall) error for aerosol scattering and absorption coefficients at all three wavelengths. Note that the data points for which the difference is larger than 30 % are discarded (*first criterion in data validation*). Once the refractive index at instruments conditions is retrieved, the dry and wet refractive indices m_{dry} and m_{wet} are determined, using a weighted mean as a function of the dry volume fraction DVF(RH) determined as the ratio between the dry volume V_{dry} and the wet volume V_{wet}:

$$\text{DVF}(\text{RH}) = \frac{V_{\text{dry}}}{V_{\text{wet}}(\text{RH})} = \frac{V_{\text{dry}}}{\text{GF}^3(\text{RH})V_{\text{dry}}} = \frac{1}{\text{GF}^3(\text{RH})} \tag{5}$$

In a first stage:

$$m_{\text{inst}} = \left[1 - \text{DVF}(\text{RH}_{\text{inst}})\right] \cdot m_{\text{water}} + (\text{RH}_{\text{inst}}) \cdot m_{\text{dry}}. \tag{6}$$

the dry refractive index is determined considering $\text{DVF}(\text{RH}_{\text{inst}})$ (Eq. 5) for GF(RH) at instruments RH conditions. The refractive index of water is a real number m_{water} =

ACPD
12, 5293–5340, 2012

1.333.

$$m_{dry} = \frac{m_{inst} - [1 - DVF(RH_{inst})] \cdot m_{water}}{DVF(RH_{inst})}. \quad (7)$$

The wet refractive index is then computed as:

$$m_{wet} = [1 - DVF(RH_{wet})] \cdot m_{water} + DVF(RH_{wet}) \cdot m_{dry}. \quad (8)$$

Here, DVF is computed for ambient (wet) RH (Eq. 5).

A second criterion in data validation is applied to the refractive index. Thus, the retrieved refractive indices at instrument conditions which reach the extremes values for the real part (i.e. 1.3 or 1.7) are discarded. A regression between the calculated and measured scattering and absorption coefficients is performed. *A third criterion* in data quality eliminates the outliers from regression analysis which correspond to the points outside 95 % confidence level.

Finally, we apply the Mie theory using the dry and wet particles diameter, particles number size distributions and refractive indices to calculate the dry and wet optical variables, respectively, and further their enhancement factors. The asymmetry parameter and its enhancement factor are calculated as well.

3.3 Error calculation

The error computation consists in a sensitivity study taking into account the errors in the input parameters. Thus, the calculations are performed once for the input parameters $x + \varepsilon_x$ and once for the input parameters $x - \varepsilon_x$. For each variable y computed along the flow chart, its relative error will be the average between the relative errors with respect to the case of $\varepsilon_x = 0$. Thus:

$$\varepsilon_y = 100 \frac{1}{2} \left(\left| \frac{y_m}{y} - 1 \right| + \left| \frac{y_p}{y} - 1 \right| \right) (\%). \quad (9)$$

y corresponds to the input parameters x ($\varepsilon_x = 0$, i.e. no error in input parameters), while y_m and y_p correspond to the input parameters $x - \varepsilon_x$ and $x + \varepsilon_x$ respectively. An

ACPD
12, 5293–5340, 2012

example of the output errors is shown in Sect. 4.3. The numerical values of the input errors are discussed in Sect. 4.3.1.

4 Results and discussions

The present study makes use of the HTDMA measurements carried out between May 2008 and February 2009 (Fig. 3). We studied the diurnal and seasonal variations in the atmospheric aerosol growth factor at 90 % RH, focusing on the data obtained in January, May, July and October (for which the data coverage was satisfactory) as representative for each season.

The monthly diurnal cycles of GF(90) observed over May 2008–February 2009 are then used as inputs in the estimation of enhancement factors over two years period (2008–2009). In order to get a complete yearly cycle of the hygroscopic growth factor, an interpolation was performed for the missing months (August, November, March and April). The procedure to determine enhancement factors needs simultaneous and consistent measurements taken by all the instruments (all the instruments mentioned as input in Fig. 1, but HTDMA for which we already determined the climatology), which was entirely fulfilled for 1062 h over the two year period. The lack of continuous exploitable measurements is mainly due to the constrain that RH inside nephelometer should be within ±5 % of that recorded in DMPS to calculate the aerosol refractive index, and second to various technical problems within different instruments.

4.1 Hygroscopic growth factor and hygroscopicity parameter

We focus on monthly averaged diurnal variations of the growth factor at 90 % RH, of which values for $d_{\mathrm{dry}} = 165$ nm is used as an input for the estimation of the enhancement factors. Figure 4 shows the diurnal GF-PDF behavior for the months of January, May, July and October, each representing a different season. GF-PDF (color scale) is shown versus dry diameter and GF. The most striking observation is the lack of diurnal

ACPD
12, 5293–5340, 2012

variations in the GF-PDF in July. During this month, a close-to-monomodal distribution is observed all the day long, with GF modes ranging from 1.1 for 35 nm particles to 1.5 for 165 nm particles. This corresponds to an aged particle population, where 35 nm particles are still mainly hydrophobic (and probably primary) while 165 nm are internal mixture of hydrophobic and hydrophilic substances, which could result from the accretion of secondary species onto hydrophobic cores. The lack of clear diurnal variations is also observed for October, but in this case the GF-PDF becomes broader and even bi-modal in most cases for particles larger than ca. 100 nm. Particles larger than 100 nm with a low (≤1.2) GF(90) are observed above all during the coldest hours of the day, and could result from the condensation of semi-volatile hydrophobic species. Indeed, these "big" (d_{dry} > 100 nm) hydrophobic particles are also observed in December, but during this month, another mode centered on a larger GF is observed for all times during the day, and for most particle diameters. As it was shown that wood burning is a major source of particulate matter in our area in winter (Gilardoni et al., 2011), we suspect these particles with a relatively high GF(90) to come from wood burning, which is know to produce a variety of water-soluble sugars (Schmidl et al., 2008). However, particles with a relatively high GF(90) (ranging from ≈1.2 for d_{dry} = 35 nm to ≈1.5 for d_{dry} = 165 nm), are also observed in May, most of the time externally mixed with purely hydrophobic particles [GF(90) ≈1], that cannot be attributed to wood burning, but rather to the mixture of hydrophobic and secondary hydrophilic aerosol and species.

The GF-PDF for each particle dry size was used to characterize the size-dependent aerosol composition following Gasparini et al. (2004) and Swietlicki et al. (2008). GF(90) for insoluble and soluble particles are assumed to be equal to the values listed in Table 1. Particles with GF(90) between these values result from a mixture of soluble and insoluble aerosol. The fractions of soluble and insoluble aerosol were calculated assuming that the GF(90) of the mixture is equal to the volume averaged mean of the purely hydrophobic and purely hydrophilic particles. Pure soluble particles were barely observed within our measurement range (up to 165 nm). Figure 5 shows that purely insoluble and mixed particles of all sizes between 35 and 165 nm co-exist at our site.

ACPD
12, 5293–5340, 2012

The fraction of soluble aerosol increases with the particle size in all four seasons.

This result is generally confirmed by the relationship between the hygroscopicity parameter (Petters and Kreidenweis, 2007) and the aerosol dry diameter. Indeed, Fig. 6 shows an increase of the hygroscopicity parameter from ca. 0.1 to 0.2 with the particle dry diameter at all times in May, July and October, which indicates a gradual increase in the particle water solubility with the particle size. As the hygroscopicity parameter was calculated from the mean GF(90), we did not capture the hygroscopicity parameter for the most hydrophilic mode in December. According to a parameterisation by Andreae and Rosenfeld (2008), the hygroscopicity parameter values of 0.1–0.2 are characteristic for moderately aged pyrogenic aerosol.

In Ispra, both growth factor and hygroscopicity parameter at RH = 90 % (Fig. 7a, b) are on average lower than in the USA (Gasparini et al., 2006), in Sweden (Fors et al., 2011), in the free troposphere at the Jungfraujoch in Switzerland (Kammerman et al., 2010), and in the China North Plain in summer (Liu et al., 2011). For D_p = 165 nm though, the mean GF(90) in Ispra is very close to that observed in Mace Head (Ireland) in polluted continental air advection conditions (Fierz-Schmidhauser et al., 2010a), Cabauw (the Netherlands) in polluted conditions with southerly flows (Zieger et al., 2011), and Beijing (China) in wintertime (Meier et al., 2009).

4.2 Retrieved parameters and enhancement factors

Besides the enhancement factors, we present the most relevant parameters determined along the intermediate calculation steps, i.e. the retrieved refractive indices, γ exponent describing GF(RH), and the aerosol asymmetry parameter.

4.2.1 Refractive indices

As mentioned in Sect. 3.2., computations were performed only for times at which the absolute difference between RH inside DMPS and RH inside nephelometer was less than 5 %. Thus, from the initial set of hourly measurements over 2008 and 2009, we

ACPD
12, 5293–5340, 2012

could lay down a number of 1062 hourly data, scattered over 84 days (mostly during winter periods). After applying the first two criteria used for data validation mentioned in Sect. 3.2 (difference between calculated and measured optical variables is smaller than 30 % and the real part of retrieved refractive index does not take extreme values), the remaining set of data includes 655 hourly data points. We did not investigate yet the reasons of discrepancy for these outliers. The linear regressions between the optical properties obtained from measurements and from the Mie computations (using the retrieved refractive indices at instruments conditions) was performed for each of the scattering, absorption and extinction coefficients (Fig. 8), and revealed 21, 81 and 19 outliers (95 % confidence level), respectively, which were discarded (*third criterion*). The combination of all three criteria finally gives us a final number of 564 cases for which we were able to reproduce the scattering, absorption and extinction coefficients at 450, 550, and 700 nm obtained from measurements, by applying the Mie theory based on wavelength-independent retrieved refractive indices, and measured particle number size distributions. This is confirmed by all three regressions (Fig. 8), for which the offset is very small, the slopes are within 6 % difference with respect to the 1:1 fit, and correlation coefficients are very good ($R^2 > 0.99$).

Refractive indices retrieved for instruments RH conditions ("inst"), dry and ambient RH conditions ("dry" and "wet") are shown in Fig. 9. Since only data taken at RH < 30 % were considered, the values at instrument conditions are very close to those in dry conditions. Both the real and imaginary part of the wet refractive index decrease with increasing RH. Note that the jump at measurement number 336 corresponds to the break between data taken in January–February 2008 (first 335 points) and the data taken in December 2008. Particles were noticeably larger in January–February 2008 compared to December 2008 (Jensen et al., 2009).

4.2.2 γ-exponent

For the 564 selected cases, 165 nm particle growth factors GF(RH), as determined by the γ-model (Eq. 4), are shown in Fig. 10. The range covered by GF(90) (1.16–1.41) is

ACPD
12, 5293–5340, 2012

quite large, and excludes only 9 % of the GF(90) values observed during the whole HTDMA measurement period. Larger GF(90) observed in summer (up to 1.48 on 10 June, 12:00 UTC) are however not accounted for. GF(RH) functions are used to determine both DVFs and particle diameters in dry and ambient conditions (Eq. 5). Then, both are used to determine the aerosol refractive indices at 0 % and ambient RH (Eqs. 7–8). The mean γ-exponent at 90 % RH is 0.12 ± 0.02. This value is much smaller than what is reported by Swietlicki et al. (2000) for the ACE-2 experiment in the Northeastern Atlantic Ocean (0.23 ± 0.01), and by Massling et al. (2003) for a study over Atlantic and Indian Oceans ($\sim 0.25 \pm 0.01$).

4.2.3 Asymmetry parameter

The linear regressions between the asymmetry parameter g retrieved from Mie calculations and from Arnott's empirical formula (Andrews et al., 2006) do not show significant correlations (Fig. 11). At instrument conditions, the average relative difference between the empirical determination and the Mie computation (Table 2) is significant with respect to uncertainties at 700 nm only (see Sect. 4.3.2). In contrast, the corresponding relative differences for the hemispherical backscatter fraction bf is larger than uncertainties for all wavelengths.

4.2.4 Enhancement factors

The enhancement factors calculated for the range of observed ambient RH for the scattering, extinction, absorption, and backscattering coefficients, the asymmetry parameter all show an increase with RH at all wavelengths (Fig. 12a–e). In contrast, the hemispherical backscatter ratio decreases with RH (Fig. 12f), since the backscatter ratio decreases with the particle size.

At λ = 550 nm, the median values of the enhancement factors at 90 ± 1 % RH for absorption, scattering, backscattering, and extinction coefficients are 1.08, 2.10, 1.67, and 1.81, respectively (Table 3, Fig. 12). The median enhancement factors for the asymmetry parameter and the backscatter fraction are 1.16 and 0.69, respectively (Table 3). These enhancement factors lead to a mean change in single scattering

ACPD
12, 5293–5340, 2012

albedo between dry and ambient conditions of 8.8 % at 550 nm. Thus, for the December–May data we analyzed, the mean and standard deviation (STD) for SSA calculated for ambient conditions was 0.84 ± 0.09, i.e. lower compared to the values reported for 550 nm at Jungfraujoch (0.95) (Fierz-Schmidhauser et al., 2010b), Mace Head (0.93) (Fierz-Schmidhauser et al., 2010a), Gosan, Korea (0.93 in polluted conditions) (Kim et al., 2006), and the Northern Indian Ocean downwind of India (0.86) (Sheridan et al., 2002).

In the literature, hygroscopic enhancement factors of the aerosol optical properties are usually reported for the scattering coefficient (Fitzgertald et al., 1982; Kotchenruther and Hobbs, 1998; Kotchenruther et al., 1999; Day and Malm, 2001; Sheridan et al., 2002; Carrico et al., 2000; Kim et al., 2008; Liu et al., 2008; Pan et al., 2009; Zieger et al., 2011) and more rarely for the backscatter coefficient (Carrico et al., 2003; Magi and Hobbs, 2003; Fierz-Schmidhauser, 2010a, b) or the absorption coefficient (e.g. Redemann et al., 2001; Nessler et al., 2005b). Most studies are based on direct measurements taken by nephelometers in dry (below 40 % RH) and wet conditions (i.e. 80 % to 90 % RH). When necessary, we calculated the scattering enhancement factors from 20–30 % to 85 % RH based on humidograms or fittings provided by the authors, so that data from various sites could be compared (Fig. 13). The mean scattering enhancement factor we observed in Ispra is among the smallest reported for Europe, but close to the values reported for Sagres (Portugal) and Mace Head (Ireland) when impacted by continental polluted air masses (Carrico et al., 2000; Fierz-Schmidhauser et al., 2010a). It is lower than the scattering enhancement factor at most other polluted sites in Asia (Carrico et al., 2003; Kim et al., 2008; Liu et al., 2008; Pan et al., 2009) or America (Fietzgerald et al., 1982; Kotchenruther et al., 1999; Day and Malm, 2001), but higher than in wood smoke plumes in South America (Kotchenruther and Hobbs, 1998), Africa (Magi and Hobbs, 2003), or Asia (Kim et al., 2008). In contrast, the backscatter ratio enhancement factor from 20–30 to 85 % in Ispra (0.80) is amongst the highest when compared to Mace Head, IR (0.80), Jungfraujoch, CH (0.72) and the Sea of Japan (0.67) (Carrico et al., 2003; Fierz-Schmidhauser et al., 2010a, b).

ACPD
12, 5293–5340, 2012

Most studies consider that the aerosol absorption coefficient does not change with RH (e.g. Nessler et. al, 2005a; Zieger et al., 2010, 2011), because absorption is usually much smaller than scattering and thus, the contribution of the absorption enhancement to the extinction enhancement is generally negligible. Based on modelling, Redemann et al. (2001) report an absorption enhancement factor at 550 nm and 90 % RH of ca. 1.15 for a monomodal size distribution that resembles what we observe at our site. From Nessler et al. (2005b) data, we estimated that the aerosol absorption enhancement factor would range at Jungfraujoch from 1.0 to 1.06 from winter to summer. The mean absorption enhancement factor (1.07 ± 0.04) we determined for Ispra based on measurements and the Mie theory is coherent with the values determined by modelling.

Nessler et al. (2005b) mention that for Jungfraujoch conditions, the contribution of the aerosol enhancement factor to extinction and SSA is about 0.2 % and thus it is discarded. Even at our site where SSA is rather low (0.77 on average at 550 nm in dry conditions), there will be a small difference (generally <1 %, up to <5 % for RH > 99 %) in estimating the extinction at ambient conditions (Fig. 14) when taking into account the humidity dependence of absorption (Eq. 10) or not (Eq. 11).

$$k_{\mathrm{wet},1} = \kappa_{\mathrm{dry}} f_{\kappa}(\mathrm{RH}) \tag{10}$$

$$k_{\mathrm{wet},2} = \sigma_{\mathrm{dry}} f_{\sigma}(\mathrm{RH}) + \alpha_{\mathrm{dry}} \tag{11}$$

Figure 15 shows regressions between $f(\mathrm{RH})$ and GF(RH) for the case of $\lambda = 550$ nm. The curves for the other two wavelengths (450 and 700 nm) are not much different (Table 4). Since the scattering, backscattering and absorption coefficients are functions of the particle area, we used second order polynomial fits. The similar behaviours of $f(\mathrm{RH})$ and GF(RH) for scattering, extinction and backscattering (Figs. 7 and 9) lead to the high correlation ($R^2 > 0.98$). The absorption enhancement factor is more scattered over the RH range ($R^2 = 0.67$), because it strongly decreases with increasing aerosol single scattering albedo. A good correlation is also found between the enhancement

ACPD
12, 5293–5340, 2012

factor for the asymmetry parameter and the backscatter ratio and the growth factor (Fig. 15).

Zieger et al. (2011) mention a good correlation ($R^2 = 0.72$) between scattering enhancement factor at 85 % RH (as determined from nephelometers measurements) and growth factor GF(90) for 165 nm. However, no further comments or correlation fit was provided.

From these correlations and the climatology for GF(RH), we can estimate the enhancement factors f_χ (with $\chi = \sigma$, α, κ, β or g) at any RH conditions for any time of the year, based on measurements of RH only. Thus, the corrected optical parameter χ at ambient condition (RH) will be given by:

$$\chi(\mathrm{RH}) = \chi(\mathrm{RH_{inst}}) \frac{f_\chi[\mathrm{GF(RH)}]}{f_\chi\left[\mathrm{GF(RH_{inst})}\right]} \quad (12)$$

The accuracy of this approach will be investigated when simultaneous measurements in wet and dry conditions of the aerosol scattering and backscattering are possible at our station.

4.3 Uncertainties

4.3.1 Uncertainties of input variables

Nephelometer calibrations (using CO_2 and zero-span) performed in 2008–2009 showed a stability within ± 1.1 %. The intercomparison performed in 2007 at the World Calibration Centre for Aerosol Physics (WCCAP) showed that our instrument measured well within the ± 5 % of the average over 10 instruments. Anderson and Ogren (1998) report particles loss within 1 % for sub-micron particles, which always largely dominate scattering at our site (see Fig. 2 as an example). The uncertainty of the corrections for non idealities is <1 %. The largest errors come from the possible growth of particles in the Nephelometer where RH is up to 30 %. The upper limit for the overall uncertainty of the scattering coefficient can thus be estimated to [−10, 0] %.

ACPD
12, 5293–5340, 2012

The aerosol absorption coefficient at 660 nm derived from the Aethalometer and nephelometer measurements were compared with the absorption coefficient at 670 nm obtained with a Multi-Angle Absorption Photometer (MAAP). MAAP instruments were shown by the WCCAP to deliver unbiased absorption coefficients in comparison with reference instruments. The correlation between hourly data obtained from the Aethalometer and the MAAP suggest an overall uncertainty of the Aethalometer derived absorption coefficient of [−10, 0] %.

Regular calibrations and intercomparisons showed that the uncertainty of the particle number size distributions obtained with our DMPS are within ±5 % in counting and ±3 % in sizing. The concentration of 600 nm (geometric diameter) particles determined from the APS and the DMPS can occasionally differ by a factor up to 3, due to measurement errors and uncertainties in the conversion from aerodynamic to geometric diameters. However, as optical properties are largely dominated by particles smaller than 600 nm (Fig. 2), such errors have no significant impact on the accuracy of the computed optical variables.

A 3 % uncertainty for GF(90) for 165 nm particles was considered, following the uncertainty during the experiments performed with ammonium sulphate for 110 nm particles. The mean standard deviation of the monthly diurnal average of GF(90) (4 %) was used for each time slot, because there were not enough points for statistics for all times and months. Thus, an overall uncertainty of 5 % is estimated for the GF(90) of 165 nm particles. At our site, the optical properties of the aerosol are dominated by 150–600 nm particles. Over the season for which enhancement factors were computed, the hygroscopic parameter does not significantly increase from 110 nm to 165 nm. We assumed that there would be no significant change from 165 nm to 600 nm either. The chemical composition of the particulate matter in the sub-2.5 µm fraction is actually consistent with the hygroscopicity observed for 165 nm particles. However, to take into account that particles larger than 165 nm could be more hydroscopic, we used a range of [0, +10] % for the uncertainty of the GF(90) values used in the computations.

ACPD
12, 5293–5340, 2012

4.3.2 Errors in retrieved parameters and computed variables

As mentioned in Sect. 3.3, the uncertainty of the retrieved parameters and computed enhancement factors is estimated through a sensitivity study. Figure 16 shows an example of the errors calculated (at 550 nm) based on data from 10 February 2009. We have chosen this particular day because RH covers a large range (from 40 % to 96 %). We can observe an increasing error with RH for all variables but the refractive index real part and the asymmetry factor.

The discussion of the uncertainties follows the flow chart (Fig. 1). The uncertainty in GF(RH), following an input error of [0, 10] % in GF(90) shows a mean ranging from 1 % (RH < 40 %) to ∼7 % at high RH (> 90 %). The real part of the refractive index shows an average uncertainty below 3 %, while the uncertainty of the imaginary part ranges from <8 % (dry) to ∼22 % at RH > 90 %. Note that the largest input error for the refractive index comes from the uncertainty in DVF which in turn, depends on $[GF(RH)]^3$. The uncertainty in dry and wet diameters is directly proportional to the uncertainty in GF(RH). The optical variables and enhancement factors have an uncertainty below 4 % at RH < 40 %, reaching 30–38 % at RH > 95 % for all but the absorption enhancement factor. The error in all enhancement factors (except absorption) depends strongly on the error in imaginary part of the refractive index. The small error for the absorption enhancement factor is due to the fact that its dependence with RH is much smaller. Similarly, for the asymmetry parameter and backscatter fraction enhancements factors, smaller errors are found (below 2 % and 7 % respectively) as their dependence on RH is relatively smaller (see Fig. 12). Andrews et al. (2006) report an uncertainty in g of 2 % corresponding to a diameter uncertainty of 5 %. Wang et al. (2002) report an absolute uncertainty of ∼25–30 % in calculating aerosol extinction (Mie Theory) taking into account the uncertainty in NSD (3 % uncertainty for size and 10 % uncertainty for number concentration). Eichler et al. (2008) report also RH dependent errors for aerosol extinction coefficient as computed by Mie theory, reaching up to 20 % at 92 % RH. Fierz-Schimdhauser (2010a) performed a sensitivity study on the prediction of the

ACPD
12, 5293–5340, 2012

scattering enhancement factor (using Mie theory). The authors found that the prediction is most sensitive to the growth factor and refractive index. Thus, for an input error of ±20 % for each of the refractive index and growth factor, the error of the scattering enhancement factor for polluted air was about [−20,+50 %] and [−40,+70 %], respectively. Therefore, the range of uncertainties we determined are consistent with previous estimates.

5 Conclusions

Aerosol hygroscopicity in terms of hygroscopic growth factor and enhancement factors of the main optical properties was determined based on measurements performed at the station for atmospheric research in Ispra and Mie calculations.

Measurements show that insoluble and mixed particles coexist at all times for all particle dry diameters at our site. The amount of water soluble matter clearly increases with the particle dry size during all seasons. We observed GF(90) values ranging from 1.16 to 1.48 for 165 nm dry diameter particles (average = 1.32 ± 0.06). A monthly diurnal cycle of the hygroscopic growth at 90 % RH was established from measurements covering 8 months within a year.

The enhancement factors for all the optical variables, i.e. aerosol scattering, absorption, extinction and backscatter coefficients, asymmetry parameter and hemispherical backscatter fraction were calculated for December–May using the Mie theory and based on input parameters retrieved from measured data. The enhancement factors for all optical coefficients but absorption strongly increase with RH. At RH = 90 % and $\lambda = 550$ nm, the aerosol scattering, extinction and absorption enhancement factors reach values of 2.1, 1.8 and 1.1 respectively (median values). The enhancement factors at 90 % RH and 550 nm for intensive variables like the asymmetry parameter and the backscatter ratio reach 1.15 and 0.78 (median), respectively. This shows that corrections for in-situ measurements taken at low RH or dry conditions are needed to get the aerosol characteristics in ambient conditions. As a strong correlation between

ACPD
12, 5293–5340, 2012

enhancement factors and growth factor was found, one can determine the corresponding enhancement factor for optical variables based on RH measurements only as soon as the seasonal-dependent diurnal cycles of the growth factor (growth factor climatology) is known. Then, measurements taken at instrument conditions for aerosol scattering and absorption can be corrected to dry and actual ambient conditions. Uncertainties estimated by performing a sensitivity study considering measurements errors in the input data demonstrated a RH-dependent uncertainty for most variables. The uncertainty of GF(90) plays an important role because the water volume fraction in particles depends on GF^3. The high uncertainty in the imaginary part of the refractive index in wet conditions (up to ca. 30 %) leads to similar uncertainties (30–38 %) in the optical variables (scattering, extinction and backscattering) and further to their enhancement factor.

Both the hygroscopicity and optical measurements performed at our station in Ispra indicate that the aerosol in our area is among the most hydrophobic and light absorbing across the world. The very good correlations between enhancement factors and hygroscopic growth factors show that the second order polynomial laws we obtained may be applied to sites with similar particle size distribution (64–124 nm mean diameter) and aerosol single scattering albedo (0.75–0.93 at 550 nm) measured in dry conditions. However, for reducing the uncertainties of these corrections, a better knowledge of the hygroscopicity of larger particles (200–500 nm) is needed.

Acknowledgements. The authors thank for the financial support of this work by the EC projects EUSAAR (contract RII3-CT-2006-026140) and ACTRIS (contract INFRA-2010-1.1.16).

References

Adam, M., Pahlow, M., Kovalev, V. A., Ondov, J. M., Parlange, M. B., and Nair, N.: Aerosol optical characterization by nephelometer and lidar: The Baltimore Supersite experiment during the Canadian forest fire smoke intrusion, J. Geophys. Res., 109, D16S02, doi:10.1029/2003JD004047, 2004.

ACPD
12, 5293–5340, 2012

Andreae, M. O. and Rosenfeld, D.: Aerosol-cloud-precipitation interactions. Part 1. The nature and sources of cloud-active aerosols, Earth Sci. Rev., 89, 13–41, 2008.

Andrews, E., Sheridan, P. J., Fiebig, M., McComiskey, A., Ogren, J. A., Arnott, P., Covert, D., Elleman, R., Gasparini, R., Collins, D., Jonsson, H., Schmid, B., and Wang, J.: Comparison of methods for deriving aerosol asymmetry parameter, J. Geophys. Res., 111, D05S04, doi:10.1029/2004JD005734, 2006.

Bohren, C. F. and Huffman, D. R.: Absorption and scattering of light by small particles, John Wiley & Sons, INC, USA, 1998.

Carrico, C. M., Rood, M. J., Ogren, J. A., Neusüß, C., Wiedensohler, A., and Heintzenberg, J.: Aerosol optical properties at Sagres, Portugal during ACE-2, 52, 694–715, 2000.

Carrico, C. M., Kus, P., Rood, M. J., Quinn, P. K., and Bates, T. S.: Mixtures of pollution, dust, sea salt, and volcanic aerosol during ACE-Asia: Radiative properties as a function of relative humidity, J. Geophys. Res, 108, 8650, doi:10.1029/2003JD003405, 2003.

Chylek, P. and Wong, J.: Effect of absorbing aerosols on global radiation budget, Geophys. Res. Lett., 22, 929–931, 1995.

Day, D. E. and Malm, W. C.: Aerosol light scattering measurements as a function of relative humidity: a comparison between measurements made at three different sites, Atmos. Environ., 35, 5169–5176, 2001.

Duplissy, J., Gysel, M., Sjogren, S., Meyer, N., Good, N., Kammermann, L., Michaud, V., Weigel, R., Martins dos Santos, S., Gruening, C., Villani, P., Laj, P., Sellegri, K., Metzger, A., McFiggans, G. B., Wehrle, G., Richter, R., Dommen, J., Ristovski, Z., Baltensperger, U., and Weingartner, E.: Intercomparison study of six HTDMAs: results and recommendations, Atmos. Meas. Tech., 2, 363–378, doi:10.5194/amt-2-363-2009, 2009.

Eichler, H., Cheng, Y. F., Birmili, W., Nowak, A., Wiedensohler, A., Brüggemann, E., Gnauk, T., Herrmann, H., Althausen, D., Ansmann, A., Engelmann, R., Tesche, M., Wendisch, M., Zhang, Y. H., Hu, M., Liu, S., and Zeng, L. M.: Hygroscopic properties and extinction of aerosol particles at ambient relative humidity in South-Eastern China, Atmos. Environ., 42, 6321–6334, 2008.

Fierz-Schmidhauser, R., Zieger, P., Vaishya, A., Monahan, C., Bialek, J., O'Dowd, C. D., Jennings, S. G., Baltensperger, U., and Weingartner E.: Light scattering enhancement factors in the marine boundary layer (Mace Head, Ireland), J. Geophys. Res., 115, D20204, doi:10.1029/2009JD013755, 2010a.

Fierz-Schmidhauser, R., Zieger, P., Gysel, M., Kammermann, L., DeCarlo, P. F., Bal-

ACPD
12, 5293–5340, 2012

tensperger, U., and Weingartner, E.: Measured and predicted aerosol light scattering enhancement factors at the high alpine site Jungfraujoch, Atmos. Chem. Phys., 10, 2319–2333, doi:10.5194/acp-10-2319-2010, 2010b.
Fitzgertald, J. W. and Hoppel, W. A.: The size and scattering of urban aerosol particles at Washington, DC, as a function of relative humidity, J. Atmos. Sci., 38, 1838–1852, 1982.
Fors, E. O., Swietlicki, E., Svenningsson, B., Kristensson, A., Frank, G. P., and Sporre, M.: Hygroscopic properties of the ambient aerosol in southern Sweden – a two year study, Atmos. Chem. Phys., 11, 8343–8361, doi:10.5194/acp-11-8343-2011, 2011.
Gasparini, R., Runjun, L., and Collins, D. R.: Integration of size distribution and size-resolved hygroscopicity measured during the Houston Supersite for compositional categorization of the aerosol, Atmos. Environ., 38, 3285–3303, 2004.
Gasparini, R., Runjun, L., Collins, D. R., Ferrare, R. A., and Brackett, V. G.: Application of aerosol hygroscopicity measured at the Atmospheric Radiation Measurement Program's Southern Great Plains site to examine composition and evolution, J. Geophys. Res., 111, D05S12, doi:10.1029/2004JD005448, 2006.
Gilardoni, S., Vignati, E., Cavalli, F., Putaud, J. P., Larsen, B. R., Karl, M., Stenström, K., Genberg, J., Henne, S., and Dentener, F.: Better constraints on sources of carbonaceous aerosols using a combined ^{14}C – macro tracer analysis in a European rural background site, Atmos. Chem. Phys., 11, 5685–5700, doi:10.5194/acp-11-5685-2011, 2011.
Gysel, M., Weingartner, E., and Baltensperger, U.: Hygroscopicity of aerosol particles at low temperatures. 2. Theoretical and experimental hygroscopic properties of laboratory generated aerosols, Environ. Sci. Technol., 36, 63–68, 2002.
Gysel, M., McFiggans, G. B., and Coe, H.: Inversion of tandem differential mobility analyser (TDMA) measurements, J. Aerosol Sci., 40, 134–151, 2009.
Jensen, N. R., Gruening, C., Adam, M., Cavalli, F., Cavalli, P., Grassi, F., Dell'Acqua, A., Martins Dos Santos, S., Roux, D., and Putaud, J.-P.: JRC Ispra EMEP – GAW regional station for atmospheric research, 2009 report, EUR 24678 EN, (2010), JRC62602, http://publications.jrc.ec.europa.eu/repository/, 2009.
Kammermann, L., Gysel, M., Weingartner, E., and Baltensperger, U.: 13-month climatology of the aerosol hygroscopicity at the free tropospheric site Jungfraujoch (3580 m a.s.l.), Atmos. Chem. Phys., 10, 10717–10732, doi:10.5194/acp-10-10717-2010, 2010.
Kasten, F.: Visibility forecast in the phase of pre-condensation, Tellus, XXI, 5, 631–635, 1969.
Kim, J., Yoon,, S.-C., Jefferson,A., and Kim, S.-W.: Aerosol hygroscopic properties during Asian

ACPD
12, 5293–5340, 2012

dust, pollution, and biomass burning episodes at Gosan, Korea in April 2001, Atmos. Environ., 40, 1550–1560, 2006.
Kotchenruther, R. A. and Hobbs, P. V.: Humidification factors of aerosols from biomass burning in Brazil, J. Geophys. Res., 103, 32081–32089, 1998.
Kotchenruther, R. A., Hobbs, P. V., and Hegg, D. A.: Humidification factors for atmospheric aerosols off the mid-Atlantic coast of the United States, J. Geophys. Res., 104, 2239–2251, 1999.
Liu, P. F., Zhao, C. S., Göbel, T., Hallbauer, E., Nowak, A., Ran, L., Xu, W. Y., Deng, Z. Z., Ma, N., Mildenberger, K., Henning, S., Stratmann, F., and Wiedensohler, A.: Hygroscopic properties of aerosol particles at high relative humidity and their diurnal variations in the North China Plain, Atmos. Chem. Phys., 11, 3479–3494, doi:10.5194/acp-11-3479-2011, 2011.
Liu, X., Cheng, Y., Zhang, Y., Jung, J., Sugimoto, N., Chang, S.-Y., Kim, Y. J., Fan, S., and Zeng, L.: Influences of relative humidity and particle chemical composition on aerosol scattering properties during the 2006 PRD campaign, Atmos. Environ., 42, 1525–1536, 2008.
Magi, B. I. and Hobbs, P. V.: Effects of humidity on aerosols in southern Africa during the biomass burning season, J. Geophys. Res., 108, 8495, doi:10.1029/2002JD002144, 2003.
Maßling, A., Wiedensohler, A., Busch, B., Neusüß, C., Quinn, P., Bates, T., and Covert, D.: Hygroscopic properties of different aerosol types over the Atlantic and Indian Oceans, Atmos. Chem. Phys., 3, 1377–1397, doi:10.5194/acp-3-1377-2003, 2003.
Meier, J., Wehner, B., Massling, A., Birmili, W., Nowak, A., Gnauk, T., Brüggemann, E., Herrmann, H., Min, H., and Wiedensohler, A.: Hygroscopic growth of urban aerosol particles in Beijing (China) during wintertime: a comparison of three experimental methods, Atmos. Chem. Phys., 9, 6865–6880, doi:10.5194/acp-9-6865-2009, 2009.
Nessler, R., Weingartner, E., and Baltensperger, U.: Adaptation of dry nephelometer measurements to ambient conditions at Jungfraujoch, Environ. Sci. Technol., 39, 2219–2228, 2005a.
Nessler, R., Weingartner, E., and Baltensperger, U.: Effect of humidity on aerosol light absorption and its implications for extinction and the single scattering albedo illustrated for a site in the lower free troposphere, J. Aerosol Sci., 36, 958–972, 2005b.
Pahlow, M., Feingold, G., Jefferson, A., Andrews, E., Ogren, J. A., Wang, J., Lee, Y.-N., Ferrare, R. A., and Turner, D. D.: Comparison between lidar and nephelometer measurements of aerosol hygroscopicity at the Southern Great Plains Atmospheric Radiation Measurement site, J. Geophys. Res., 111, D005S15, doi:10.1029/2004JD005646, 2006.

ACPD
12, 5293–5340, 2012

Pan, X. L., Yan, P., Tang, J., Ma, J. Z., Wang, Z. F., Gbaguidi, A., and Sun, Y. L.: Observational study of influence of aerosol hygroscopic growth on scattering coefficient over rural area near Beijing mega-city, Atmos. Chem. Phys., 9, 7519–7530, doi:10.5194/acp-9-7519-2009, 2009.

Petters, M. D. and Kreidenweis, S. M.: A single parameter representation of hygroscopic growth and cloud condensation nucleus activity, Atmos. Chem. Phys., 7, 1961–1971, doi:10.5194/acp-7-1961-2007, 2007.

Redemann, J., Russell, P. B., and Hamill, P.: Dependence of aerosol light absorption and single-scattering albedo on ambient relative humidity for sulfate aerosols with black carbon cores, J. Geophys. Res., 106, 27485–27495, 2001.

Schmid, O., Artaxo, P., Arnott, W. P., Chand, D., Gatti, L. V., Frank, G. P., Hoffer, A., Schnaiter, M., and Andreae, M. O.: Spectral light absorption by ambient aerosols influenced by biomass burning in the Amazon Basin. I: Comparison and field calibration of absorption measurement techniques, Atmos. Chem. Phys., 6, 3443–3462, doi:10.5194/acp-6-3443-2006, 2006.

Schmidhauser, R., Zieger, P., Weingartner, E., Gysel, M., DeCarlo, P. F., and Baltensperger, U: Aerosol light scattering at high relative humidity at a high alpine site (Jungfraujoch), European Aerosol Conference, Karlsruhe, Germany, 6–11 September 2009, T047A07, 2009.

Schmidl, C., Marr, I. L., Caseiro, A., Kotianova, P., Berner, A., Bauer, H., Kasper-Giebl, A., and Puxbaum, H.: Chemical characterisation of fine particle emissions from wood stove combustion of common woods growing in mid-European Alpine regions, Atmos. Environ., 42, 126–141, 2008.

Sheridan, P. J., Jefferson, A., and Ogren, J. A.: Spatial variability of submicrometer aerosol radiative properties over the Indian Ocean during INDOEX, J. Geophys. Res., 107, 8011, doi:10.1029/2000JD000166, 2002.

Swietlicki, E., Jingchuan, Z., Berg, O. H., Martinsson, B. G., Frank, G., Cederfelt, S.-E., Dusek, U., Berner, A., Birmili, W., Wiedensohler, A., Yuskiewicz B., and Bower, K. N.: A closure study of sub-micrometer aerosol particle hygroscopic behaviour, Atmos. Res., 50, 205–240, 1999.

Swietlicki, E., Zhou, J., Covert, D. S., Hämeri, K., Busch, B., Väkeva, M., Dusek, U., Berg, O. H., Wiedensohler, A., Aalto, P., Mäkelä, J., Martinsson, B. G., Papaspiropoulos, G., Mentes, B., Frank, G., and Stratmann, F.: Hygroscopic properties of aerosol particles in the northeastern Atlantic during ACE-2, Tellus B, 52, 201–227, 2000.

Swietlicki, E., Hansson, H.-C., Hämeri, K., Svenningsson, B., Massling, A., Mcfiggans, G., Mcmurry, P. H., Petäjä, T., Tunved, P., Gysel, M., Topping, D., Weingartner, E., Baltensperger,

ACPD
12, 5293–5340, 2012

U., Rissler, J., Wiedensohler, A., and Kulmala, M.: Hygroscopic properties of submicrometer atmospheric aerosol particles measured with H-TDMA instruments in various environments – A review, Tellus B, 60B, 432–469, 2008.

Swietlicki, E., Fors, E., Gysel, M., Weingartner, E., Baltensperger, U., Kammermann, L., Laj, P., Ehn, M., Mikkilä, J., Petäjä, T., Kulmala, M., Kinder, F., Kaaden, N., Wiedensohler, A., Hyvärinen, A.-P., Lihavainen, H., Kerminen, V.-M., Good, N., Michaud, V., Sellegri, K., Adam, M., Grüning, C., Putaud, J.-P., McFiggans, G., Bialek, J., O'Dowd, C., Ondracek, J., Smolik, J., Hennig, T., Hansson, H.-C., and Fjäraa, A. M.: Hygroscopic Properties of Sub-Micrometer Atmospheric Aerosol Particles from Long-term Measurements with H-TDMA Instruments across Europe 2008–2009, to be submitted to Atmos. Chem. Phys., 2012.

Topping, D. O., McFiggans, G. B., and Coe, H.: A curved multi-component aerosol hygroscopicity model framework: Part 1 – Inorganic compounds, Atmos. Chem. Phys., 5, 1205–1222, doi:10.5194/acp-5-1205-2005, 2005.

Van de Hulst, H. C.: Light scattering by small particles, Dover Publications, INC., New York, 1981.

Van Dingenen, R., Putaud, J.-P., Martins-Dos Santos, S., and Raes, F.: Physical aerosol properties and their relation to air mass origin at Monte Cimone (Italy) during the first MINATROC campaign, Atmos. Chem. Phys., 5, 2203–2226, doi:10.5194/acp-5-2203-2005, 2005.

Virkkula, A., Van Dingenen, R., Raes, F., and Hjorth, J.: Hygroscopic properties of aerosol formed by oxidation of limonene, α-pinene, and β-pinene, J. Geophys. Res., 104, 3569–3579, 1999.

Wang, J., Flagan, R. C., Seinfeld, J. H., Jonsson, H. H., Collins, D. R., Russell, P. Bb, Schmid, B., Redemann, J., Livingston, J. M., Gao, S., Hegg, D. A., Welton, E. J., and Bates D.: Clear-column radiative closure during ACE-Asia: Comparison of multiwavelength extinction derived from particle size and composition with results from Sun photometry, J. Geophys. Res., 107, 4688, doi:10.1029/2002JD002465, 2002.

Weingartner, E., Saatho, H., Schnaiter, M., Streit, N., Bitnar, B., and Baltensperger, U.: Absorption of light by soot particles: determination of the absorption coefficient by means of aethalometers, J. Aerosol Sci., 34, 1445–1463, 2003.

Zieger, P., Fierz-Schmidhauser, R., Gysel, M., Ström, J., Henne, S., Yttri, K. E., Baltensperger, U., and Weingartner, E.: Effects of relative humidity on aerosol light scattering in the Arctic, Atmos. Chem. Phys., 10, 3875–3890, doi:10.5194/acp-10-3875-2010, 2010.

Zieger, P., Weingartner, E., Henzing, J., Moerman, M., de Leeuw, G., Mikkilä, J., Ehn, M.,

ACPD
12, 5293–5340, 2012

Petäjä, T., Clémer, K., van Roozendael, M., Yilmaz, S., Frieß, U., Irie, H., Wagner, T., Shaiganfar, R., Beirle, S., Apituley, A., Wilson, K., and Baltensperger, U.: Comparison of ambient aerosol extinction coefficients obtained from in-situ, MAX-DOAS and LIDAR measurements at Cabauw, Atmos. Chem. Phys., 11, 2603–2624, doi:10.5194/acp-11-2603-2011, 2011.

ACPD
12, 5293–5340, 2012

Table 1. Maximum and minimum limits for delimitation of pure hydrophobic and pure hydrophilic particles, respectively.

d_{dry} (nm)	GF(90) upper limit for pure hydrophobic particles	GF(90) lower limit for pure hydrophilic particles
35	1.09	1.78
50	1.10	1.81
75	1.11	1.84
110	1.11	1.86
165	1.12	1.87

ACPD
12, 5293–5340, 2012

Table 2. Asymmetry parameter.

$< g >$ ± STD	450 nm	550 nm	700 nm
Nephelometer (instrument conditions)	0.60 ± 0.05	0.57 ± 0.05	0.48 ± 0.06
Mie (instrument conditions)	0.63 ± 0.04	0.59 ± 0.04	0.53 ± 0.04
Mie (ambient conditions)	0.68 ± 0.05	0.64 ± 0.06	0.59 ± 0.06

ACPD
12, 5293–5340, 2012

Table 3. Enhancement factor for optical variables (absorption – α , scattering – σ, backscattering – β, extinction – κ, asymmetry parameter – g and backscatter fraction – bf) at 90 ± 1 % RH. Also shown, single scattering albedo (SSA).

f(RH)	450 nm	550 nm	700 nm
α min	0.99	1.02	1.05
max	1.21	1.19	1.18
median	1.07	1.08	1.10
σ min	1.55	1.58	1.62
max	2.95	3.00	3.07
median	2.05	2.10	2.17
β min	1.34	1.33	1.34
max	1.97	1.95	1.99
median	1.76	1.67	1.66
κ min	1.44	1.44	1.44
max	2.03	2.08	2.12
median	1.79	1.81	1.84
g min	1.09	1.10	1.12
max	1.19	1.20	1.21
median	1.13	1.16	1.18
bf min	0.62	0.63	0.65
max	0.78	0.78	0.81
median	0.69	0.69	0.71
SSA min	0.59	0.56	0.51
max	0.93	0.92	0.91
median	0.85	0.83	0.81

ACPD
12, 5293–5340, 2012

Table 4. Regression analysis between enhancement factors f(RH) and growth factor GF(RH).

λ f(RH)	450 nm	550 nm	700 nm
σ R^2 fit	0.98 $3.92GF^2-5.97GF+3.06$	0.981 $4.75GF^2-7.81GF+4.08$	0.982 $5.89GF^2-10.3GF+5.43$
κ R^2 fit	0.991 $3.19GF^2-5.01GF+2.83$	0.990 $3.78GF^2-6.34GF+3.59$	0.987 $4.44GF^2-7.85GF+4.46$
β R^2 fit	0.973 $3.12GF^2-5.27GF+3.18$	0.984 $3.28GF^2-5.86GF+3.62$	0.983 $3.04GF^2-5.31GF+3.3$
α R^2 fit	0.545 $-0.153GF^2+0.564GF+0.583$	0.665 $-0.181GF^2+0.662GF+0.515$	0.797 $-0.218GF^2+0.796GF+0.419$
g R^2 fit	0.942 $-0.369GF^2+1.27GF+0.0968$	0.956 $-0.37GF^2+1.34GF+0.0327$	0.963 $-0.33GF^2+1.32GF+0.0076$
bf R^2 fit	0.990 $0.794GF^2-2.77GF+2.97$	0.994 $0.675GF^2-2.49GF+2.8$	0.988 $0.475GF^2-1.96GF+2.47$

σ, κ, β, α, g, bf stand for aerosol scattering, extinction, backscattering, absorption coefficients, aerosol asymmetry parameter and aerosol backscatter fraction.

ACPD
12, 5293–5340, 2012

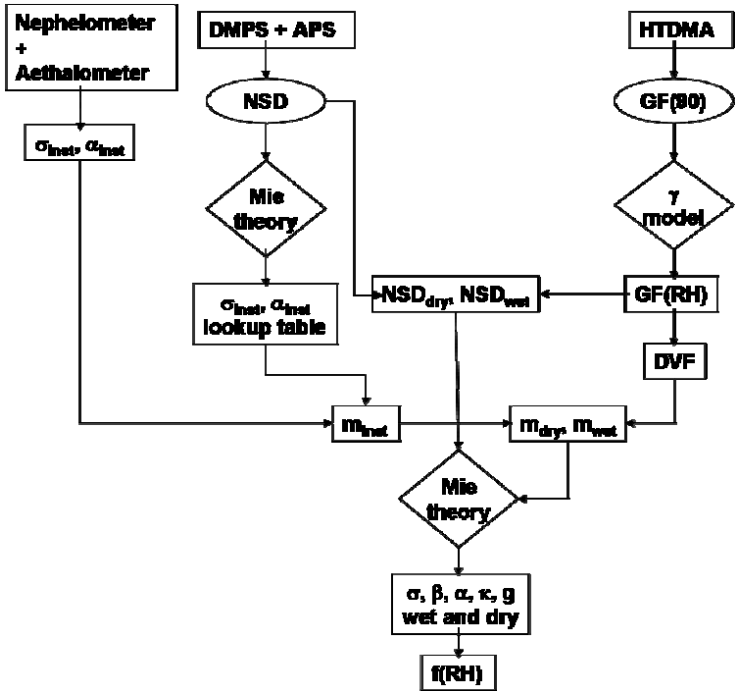

Fig. 1. Flow chart to estimate the enhancement factors. The acronyms are as follows: NSD = particle number size distribution, σ_{inst} = aerosol scattering coefficient provided by nephelometer, α_{inst} = aerosol absorption coefficient derived from aethalometer, GF(90) = average GF (monthly diurnal) for 165 nm at RH = 90 %, m_{inst}, m_{dry}, m_{wet} = refractive index at instruments RH, RH = 0 % and ambient RH, DVF = dry volume fraction, f(RH) = enhancement factor, σ, β, α, κ, g = aerosol scattering, absorption, backscatter, extinction coefficients and aerosol asymmetry parameter calculated with Mie theory.

ACPD
12, 5293–5340, 2012

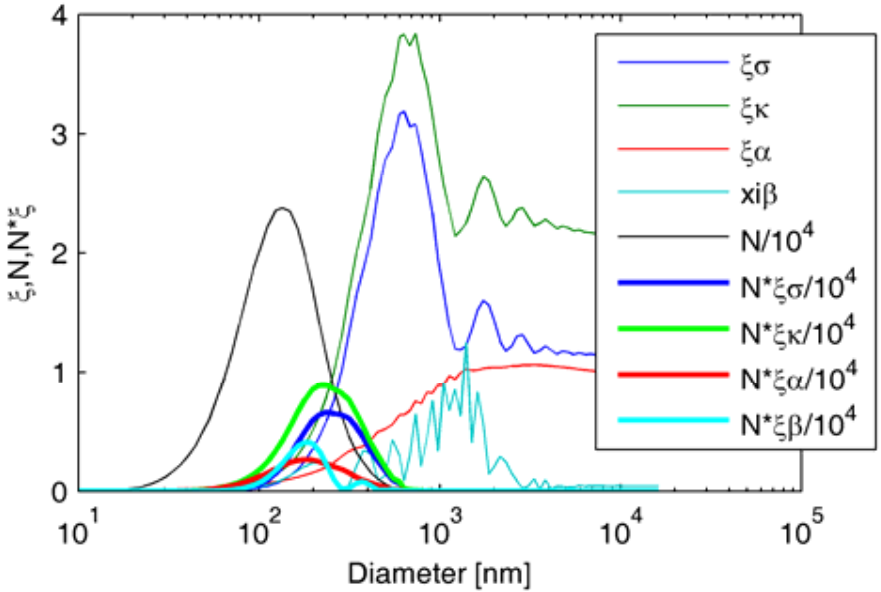

Fig. 2. Efficiency – ξ (for scattering – σ, extinction – κ, absorption – α and backscattering – β), particle number concentration (N) and the contributions to scattering, extinction, absorption, and backscattering ($N \cdot \xi$) for each diameter (λ = 550 nm). N was recorded on 10 February 2008, 05:00 UTC.

ACPD
12, 5293–5340, 2012

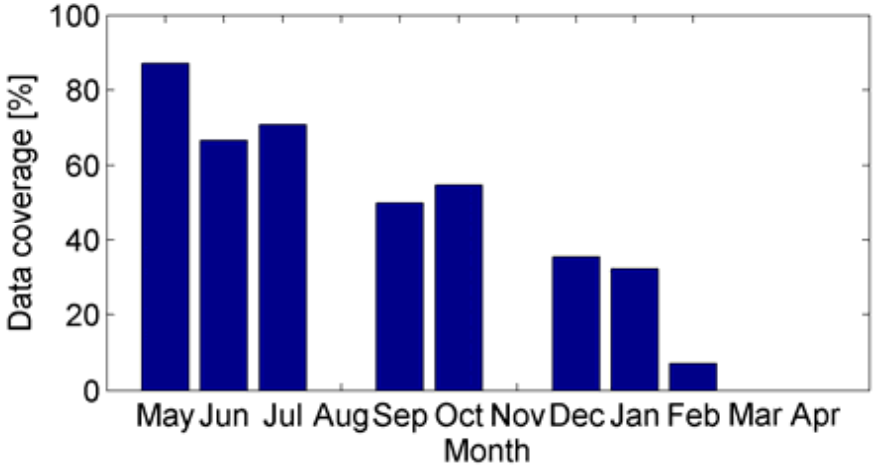

Fig. 3. Data coverage for HTDMA measurements during 2008–2009.

ACPD
12, 5293–5340, 2012

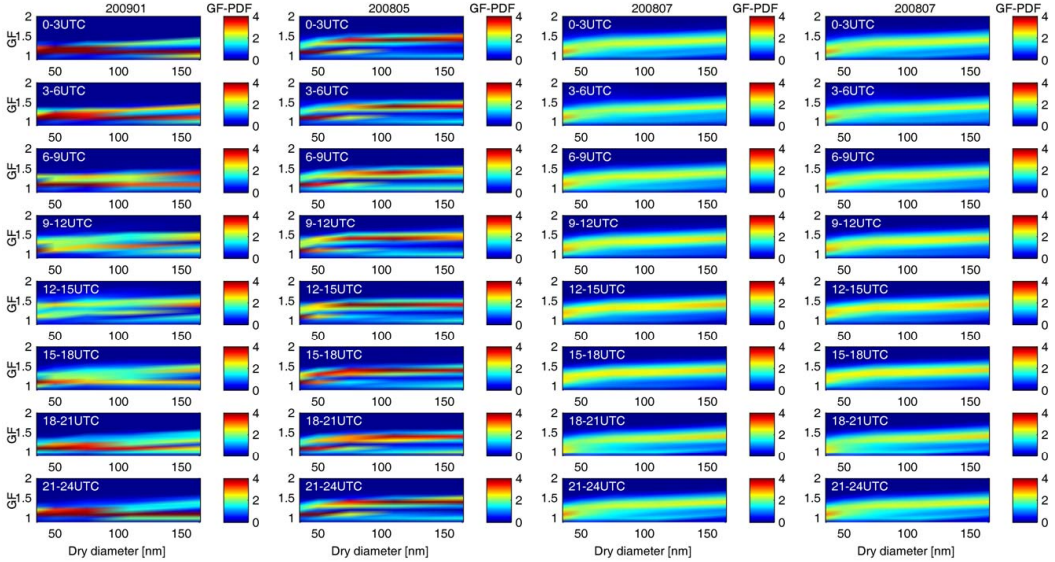

Fig. 4. GF-PDF versus GF and dry diameter for January 2009, May 2008, July 2008 and October 2008.

ACPD
12, 5293–5340, 2012

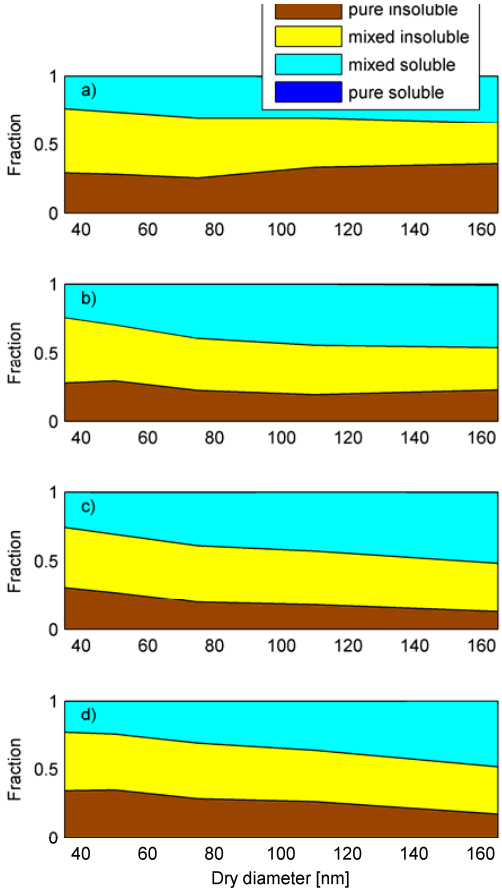

Fig. 5. Aerosol composition by dry diameter, as determined by the GF-PDF, for January 2009 **(a)**, May 2008 **(b)**, July 2008 **(c)** and October 2008 **(d)**.

ACPD
12, 5293–5340, 2012

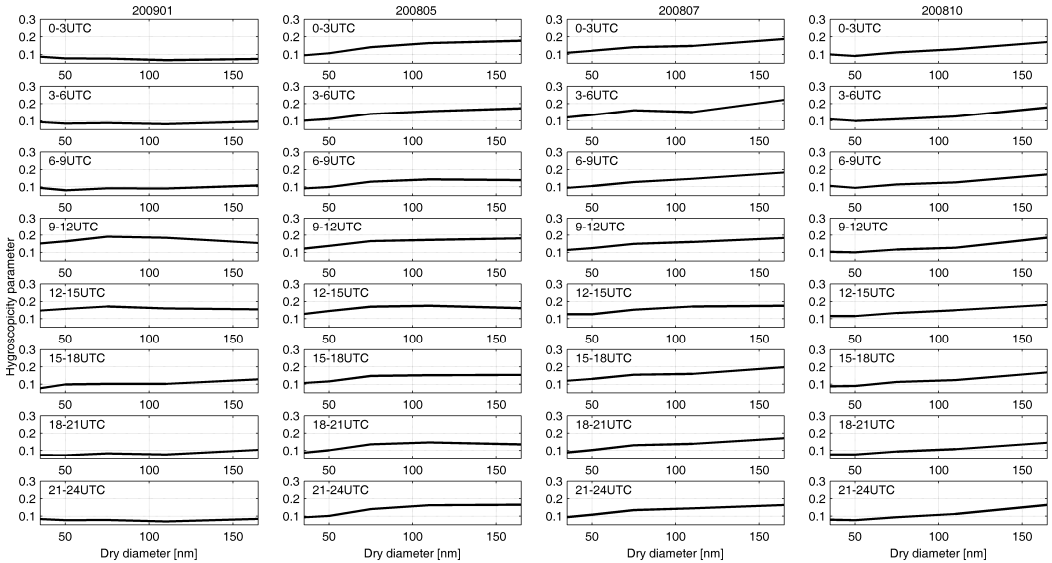

Fig. 6. Hygroscopicity parameter versus dry diameter for January 2009, May 2008, July 2008 and October 2008.

ACPD
12, 5293–5340, 2012

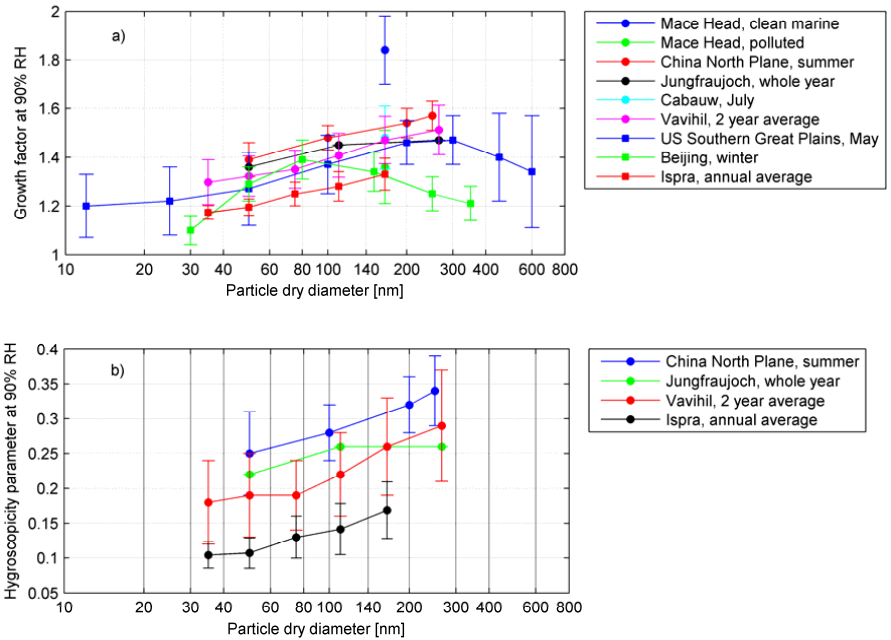

Fig. 7. Average and standard deviation of hygroscopic growth factor GF(RH) **(a)** and hygroscopicity parameter **(b)** at 90 % RH observed at various sites across the world (see references in Sect. 4.1).

ACPD
12, 5293–5340, 2012

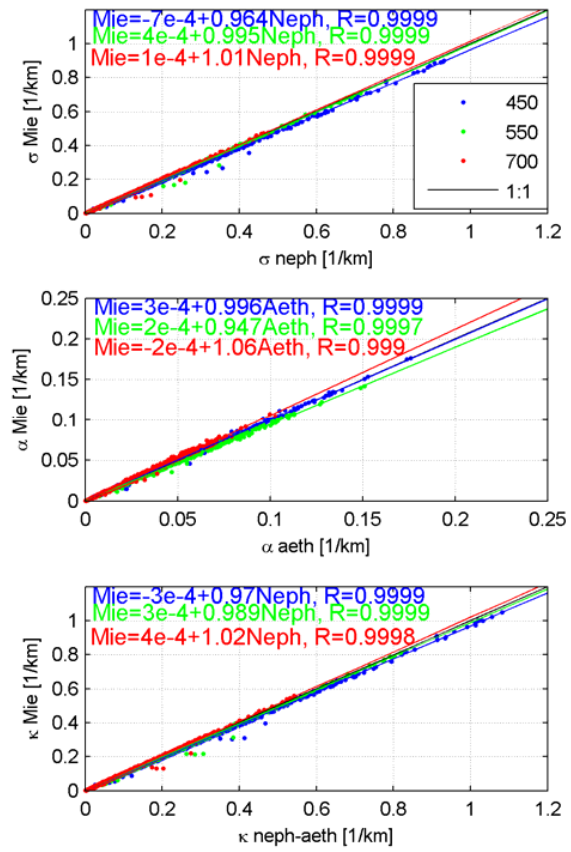

Fig. 8. Linear regression between computed (Mie) and measured aerosol scattering **(a)**, absorption **(b)** and extinction **(c)** coefficients, for all three wavelengths 450, 550, and 700 nm. The regression lines (from which outliers are excluded) and 1:1 line are shown as well. Note that, in the figure captions, "Neph" and "Aeth" stand for nephelometer and aethalometer, respectively.

ACPD
12, 5293–5340, 2012

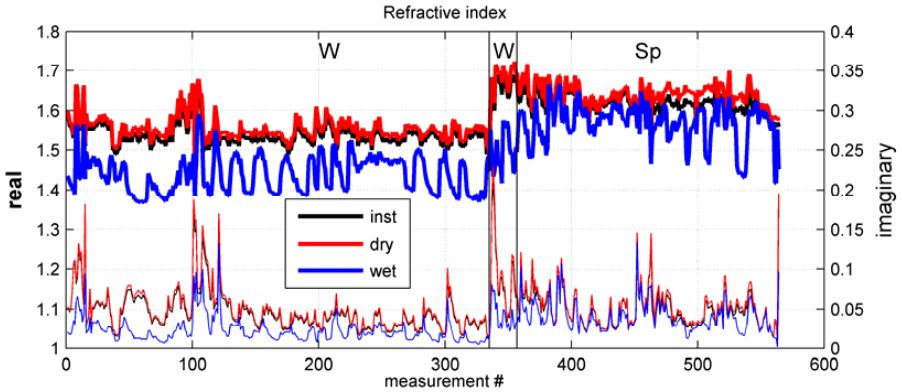

Fig. 9. Refractive index. Thick lines represent the real part (left axis) while thin lines show the imaginary part (right axis). The vertical black lines make the delimitation between different seasons (W = winter, Sp = spring).

ACPD
12, 5293–5340, 2012

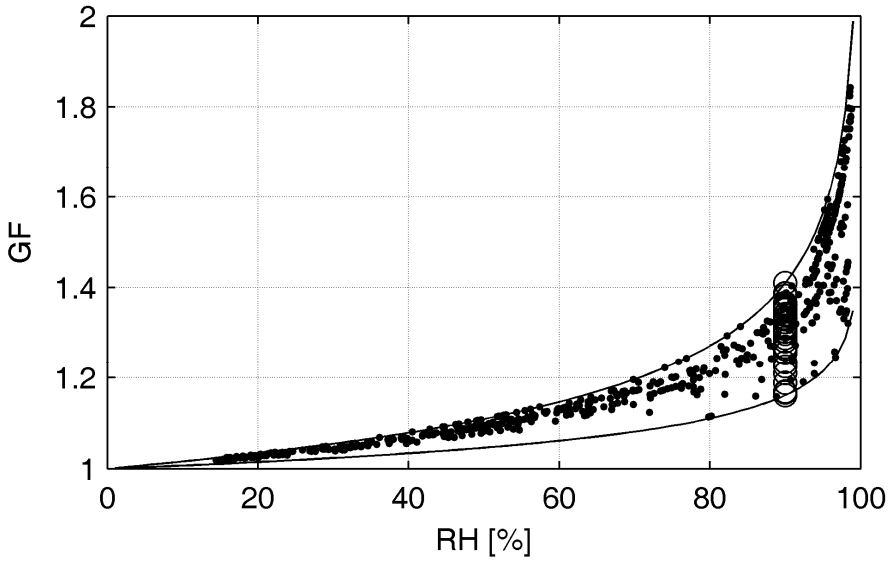

Fig. 10. Growth factors GF(RH) for 165 nm dry diameter over the whole RH range, as estimated from the γ law (Eq. 4) and GF(90) measured for the 564 selected events (circles). Also shown (lines) are the γ functions corresponding to the smallest and the largest GF(90) values.

ACPD
12, 5293–5340, 2012

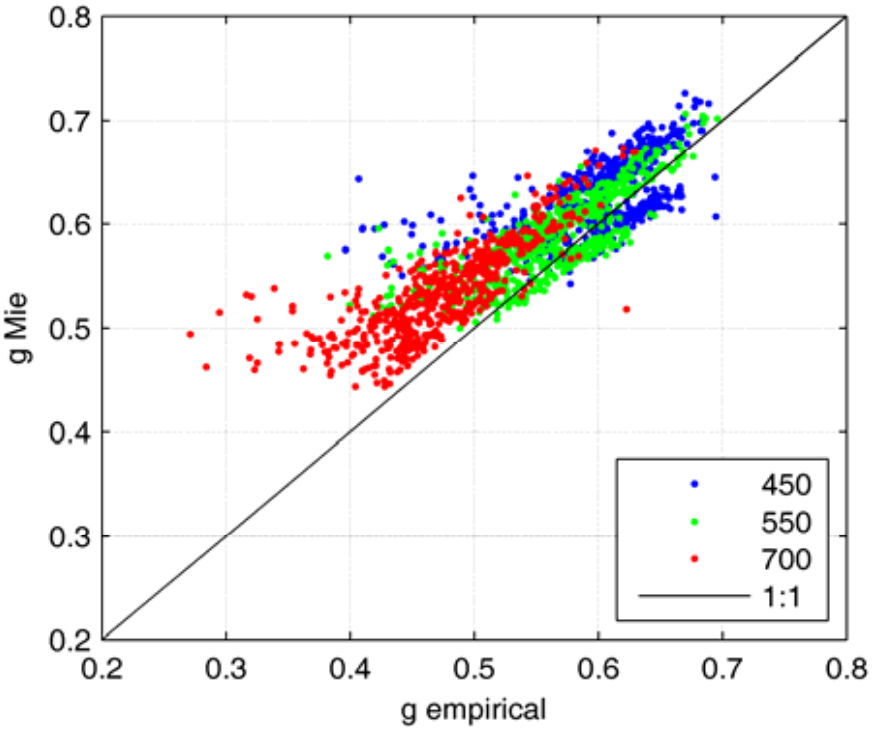

Fig. 11. Regressions between the asymmetry factors calculated from Mie theory and the empirical formula from Andrews et al. (2006) for 450, 550, and 700 nm.

ACPD
12, 5293–5340, 2012

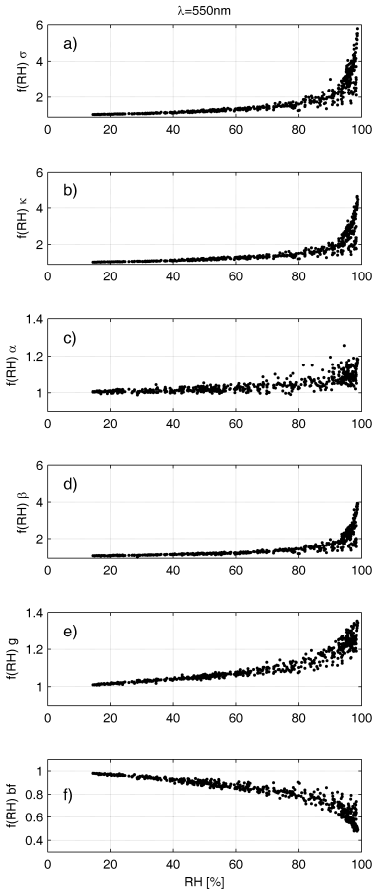

Fig. 12. Enhancement factors for aerosol scattering **(a)**, extinction **(b)**, absorption **(c)** and backscatter **(d)** coefficients, asymmetry parameter **(e)** and backscatter fraction **(f)** at 550 nm.

ACPD
12, 5293–5340, 2012

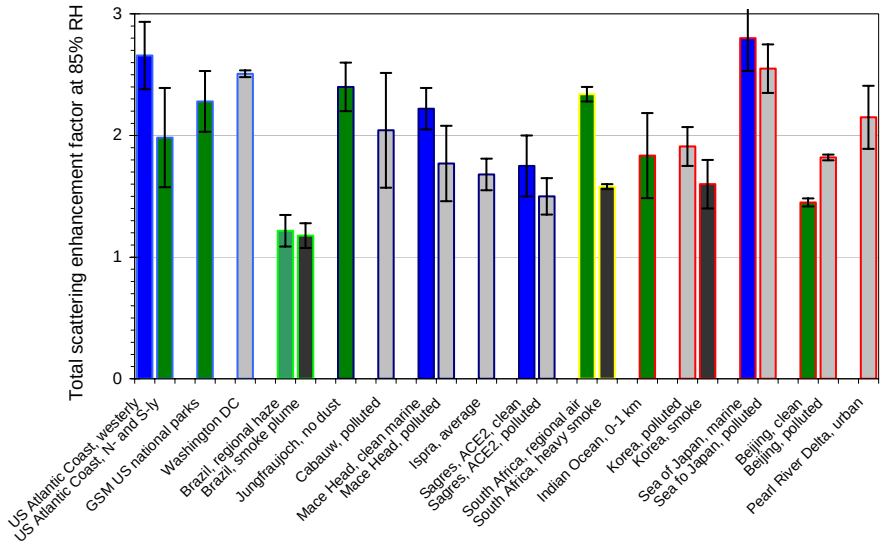

Fig. 13. Scattering enhancement factor between 20–30 % and 85 % RH from various sites (see references in Sect. 4.2.4).

ACPD
12, 5293–5340, 2012

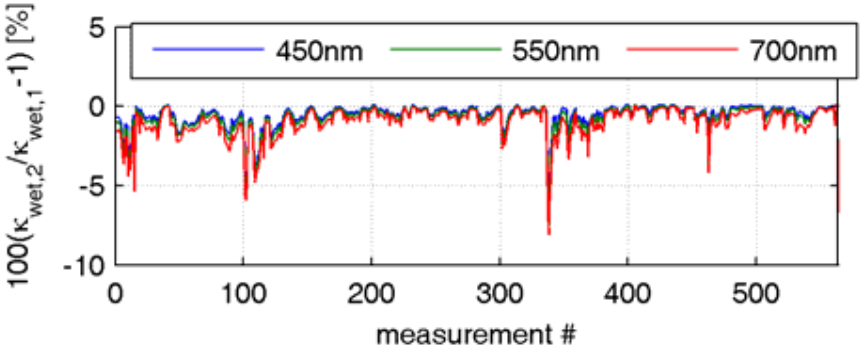

Fig. 14. The relative error in estimating the wet aerosol extinction coefficient assuming that absorption does not depend on RH.

ACPD
12, 5293–5340, 2012

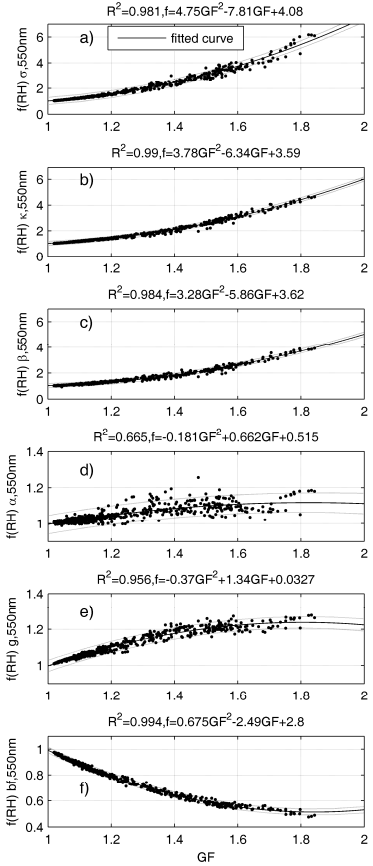

Fig. 15. Regression analysis between enhancement factors f(RH) and GF(RH), at 550 nm, for scattering coefficient **(a)**, extinction coefficient **(b)**, backscatter coefficient **(c)**, absorption coefficient **(d)**, asymmetry parameter **(e)** and backscatter fraction **(f)**. The dotted curves represent the 95 % confidence level of the fitted curves.

ACPD
12, 5293–5340, 2012

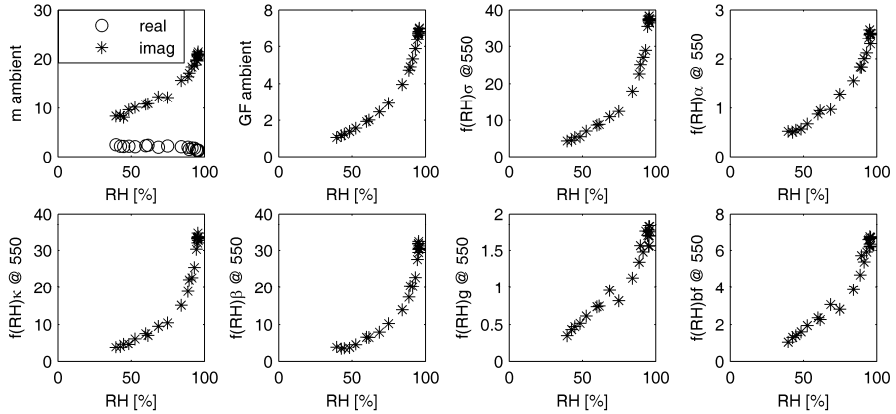

Fig. 16. The RH dependence of the uncertainty (%) for the retrieved refractive index, growth factor (GF), and computed enhancement factors f(RH) for the scattering (σ), absorption (α), extinction (κ), backscattering (β) coefficients, the asymmetry parameter (g) and the backscatter fraction (bf).

ACPD
12, 5293–5340, 2012